Bioactive Materials 6 (2021) 3343–3357

Contents lists available at ScienceDirect

Bioactive Materials

journal homepage: www.sciencedirect.com/journal/bioactive-materials

Protective effects of sirtuin 3 on titanium particle-induced osteogenic inhibition by regulating the NLRP3 inflammasome via the GSK-3β/β-catenin signalling pathway

Kai Zheng [a,1], Jiaxiang Bai [a,1], Ning Li [a,1], Meng Li [a,b,1], Houyi Sun [a], Weicheng Zhang [a], Gaoran Ge [a], Xiaolong Liang [a], Huaqiang Tao [a], Yi Xue [d], Yuefeng Hao [e,****], Chen Zhu [b,***], Yaozeng Xu [a,**], Dechun Geng [a,c,*]

[a] Department of Orthopaedics, The First Affiliated Hospital of Soochow University, No. 188 Shizi Street, Suzhou, Jiangsu, 215006, PR China
[b] Department of Orthopaedics, The First Affiliated Hospital of USTC, Division of Life Sciences and Medicine, University of Science and Technology of China, Lujiang Road No. 17, Hefei, Anhui, 230001, PR China
[c] Jiangsu Key Laboratory of Clinical Immunology, Soochow University, No. 708 Renmin Road, Suzhou, Jiangsu, 215007, PR China
[d] Department of Orthopaedics, Changshu Hospital Affiliated to Nanjing University of Traditional Chinese Medicine, Suzhou, Jiangsu, 215500, PR China
[e] Orthopaedics and Sports Medicine Center, Suzhou Municipal Hospital (North District), Nanjing Medical University Affiliated Suzhou Hospital, No. 242 Guangji Road, Suzhou, 215006, PR China

ARTICLE INFO

Keywords:
SIRT3
Titanium particles
Periprosthetic osteolysis
NLRP3 inflammasome
Osteoblast

ABSTRACT

Periprosthetic osteolysis (PPO) remains the key factor in implant failure and subsequent revision surgery and is mainly triggered by wear particles. Previous studies have shown that inhibition of osteoblastic differentiation is the most widespread incident affecting the interface of trabecular and loosening prostheses. Additionally, the NLRP3 inflammasome is activated by prosthetic particles. Sirtuin3, an NAD^+-dependent deacetylase of mitochondria, regulates the function of mitochondria in diverse activities. However, whether SIRT3 can mitigate wear debris-induced osteolysis by inhibiting the NLRP3 inflammasome and enhancing osteogenesis has not been previously reported. Therefore, we investigated the role of SIRT3 during the process of titanium (Ti) particle-induced osteolysis. We revealed that upregulated SIRT3 dramatically attenuated Ti particle-induced osteogenic inhibition through suppression of the NLRP3 inflammasome and improvement of osteogenesis *in vivo* and *in vitro*. Moreover, we found that SIRT3 interference in the process of Ti particle-induced osteolysis relied on the GSK-3β/β-catenin signalling pathway. Collectively, these findings indicated that SIRT3 may serve as a rational new treatment against debris-induced PPO by deacetylase-dependent inflammasome attenuation.

1. Introduction

Total joint arthroplasties (TJAs) are common surgical procedures that have considerable success in alleviating pain and restoring joint function for patients suffering from end-stage arthritis. As the aging and obesity population is rapidly rising worldwide, the incidence of TJAs is dramatically increasing as well, which creates a substantial clinical and economic public health burden. It is predicted that the number of revision surgeries will significantly increase given the large volume of total joint arthroplasties [1]. According to Joint Replacement Registry data, aseptic loosening is the leading aetiology for revision surgery, accounting for 24.6% of cases in Australia and 20.3% of cases in the USA [2,3]. The key factor triggering aseptic loosening and subsequent periprosthetic osteolysis (PPO) is the accumulation of wear particles around the implant, such as titanium (Ti) particles [4]. Moreover, the disruption of bone homeostasis by wear particles leads to osteoclast activation and

Peer review under responsibility of KeAi Communications Co., Ltd.
* Corresponding author. Department of Orthopaedics, The First Affiliated Hospital of Soochow University, No. 188 Shizi Street, Suzhou, Jiangsu, 215006, PR China
** Corresponding author.
*** Corresponding author.
**** Corresponding author.
E-mail addresses: 13913109339@163.com (Y. Hao), zhuchena@ustc.edu.cn (C. Zhu), xuyaozeng@163.com (Y. Xu), szgengdc@suda.edu.cn (D. Geng).
[1] These authors contributed equally to this work.

https://doi.org/10.1016/j.bioactmat.2021.02.039
Received 5 November 2020; Received in revised form 23 February 2021; Accepted 26 February 2021

osteoblast inhibition, resulting in PPO [5,6]. Consequently, partial bone around the implant is devastated, and bone integrity is destroyed. The inhibition of osteogenic differentiation was identified as the most widespread incident affecting the surface of trabecular and loosening prostheses [7], while traditional anti-osteoporosis drugs such as bisphosphonates, calcitonin, raloxifene, and denosumab mainly focus on preventing the bone resorption caused by osteoclasts [8–12]. In addition, lytic bone cannot be restored even when osteoclasts are controlled. Therefore, another factor, osteoblasts, which regulate bone formation, represent an attractive candidate therapeutic target for osteolysis.

SIRT3 (Sirtuin3), one of the members of the sirtuin family, is an NAD^+-dependent protein deacetylase located in the mitochondria [13]. Accumulating evidence indicates that SIRT3 is involved in a wide variety of beneficial activities, including antioxidation, regulation of energy metabolism, antidegeneration and antitumour activities, by regulating mitochondria-derived reactive oxygen species (ROS) and the electron transfer chain [13–15]. Recently, several studies have revealed that SIRT3 regulates bone homeostasis. SIRT3 might function as a negative regulator of osteoclast differentiation via the AMPK-PGC-1β axis [16]. Moreover, Kim et al. observed that SIRT3 controls osteoclastogenesis by activating superoxide dismutase 2 (SOD2) and regulating mitochondrial ROS [17]. For osteoblasts, SIRT3 was reported to promote osteogenic differentiation through the PGC-1α-SOD2 pathway [18]. Collectively, SIRT3 has been identified as a positive factor in bone remodelling. Nevertheless, whether SIRT3 improves wear particle-induced osteolysis by enhancing osteogenesis has not been reported.

Pyroptosis is defined as a process of programmed inflammatory cell death associated with several specific factors, including NLRP3 (NLR family pyrin domain containing 3), gasdermin D (GSDMD) and caspase-1 [19]. The NLRP3 inflammasome is a complex that contains the NLR sensor protein, adaptor protein ACS and effector pro-caspase-1 [20], which recognize multiple sets of tissue damage stimuli and control the secretion of the proinflammatory cytokines interleukin-1β and 18 [21]. Thus, the NLRP3 inflammasome is activated and assembled by stimulation via wear particles, acting through IL-1β to increase osteoclastic bone resorption [22,23]. In addition, investigation of the relationship between NLRP3 and SIRT3 revealed that depletion of SIRT3 enhanced NLRP3 inflammasome activation accompanied by excessive ROS production [24]. However, whether SIRT3 could regulate the NLRP3 inflammasome to attenuate wear particle-induced periprosthetic osteolysis is unclear.

In this study, we determined the function of SIRT3 in the process of Ti particle-induced periprosthetic osteolysis and explored possible mechanisms using rat-mesenchymal stem cells (rMSCs) *in vitro* and a Ti particle-mediated peri-implant osteolysis model *in vivo*. We demonstrated that bone loss surrounding the implant would be inhibited by upregulating the expression of SIRT3 to enhance osteogenic differentiation through regulation of the NLRP3 inflammasome via GSK-3β/β-catenin signalling. Our findings may provide new insights into treatment against wear debris-induced PPO to alleviate aseptic loosening by deacetylase-dependent inflammasome attenuation.

2. Materials and methods

2.1. Collection of clinical samples

All procedures for clinical sample collection and utilization received permission from the Bioethics Committee of the First Affiliated Hospital of Soochow University, and informed consent was obtained from patients. All samples were collected from two groups of patients (n = 3 per group). One group had osteoarthritis and underwent primary TJA, and the other group had TJA previously but needed revision surgery due to aseptic loosening. We only collected the discarded tissues resected from the joint capsule, which caused no additional harm to individuals.

2.2. Preparation of titanium particles and rods

Ti particles were obtained from Alfa Aesar (Ward Hill, MA), of which over 90% had diameters less than 4 μm [25]. Endotoxins were eliminated by soaking in 75% alcohol for 2 days, rinsing three times with sterile ultrapure water, and then burning at 180 °C for 12 h. The concentration of endotoxins in particles was detected by Limulus assay (LAL, Biowhittaker, USA) to ensure that the endotoxin levels were less than 0.02 EU/ml. Then, the Ti particles were stored with sterile PBS at 4 °C until use. Ti rods were purchased from Sigma (St. Louis, USA) and were 10 mm in length and 1.5 mm in diameter. Ti rods were sterilized using autoclaving and etched by piranha solution (95–98% H_2SO_4 and 30% H_2O_2 with 3:1 vol mixed); subsequently, the rods were deposited under sterile conditions.

2.3. Animals and peri-implant osteolysis induction

Experimental procedures were authorized by the Animal Ethics Committee of the First Affiliated Hospital of Soochow University and met the guidelines of the Care and Use of Laboratory Animals. A total of 40 twelve-week-old male Sprague-Dawley rats with an average weight of 300 ± 30 g were used. Before surgery, all rats received intraperitoneal (i.p.) injection of 2% pentobarbital sodium anaesthesia at a dose of 0.02 ml/10 g. The bilateral knee was disinfected and prepared for intramedullary Ti rod implantation in the femoral canal of the rat. A 100 μl 0.1 mg/ml Ti particle suspension was infused into the marrow cavity before implanting the Ti rod with preliminary fixation and then suturing and closing the incision. In brief, 40 rats were randomly classified into four groups (n = 10 each group): the control group (implant + SIRT3-shRNA NC (negative control) lentivirus), vehicle group (implant + Ti particles + SIRT3-shRNA NC lentivirus), LV-SIRT3 group (implant + Ti particles + SIRT3-overexpression lentivirus) and LV-shSIRT3 group (implant + Ti particles + SIRT3-shRNA lentivirus). The LV-SIRT3 and LV-shSIRT3 groups received intramuscular (i.m.) administration of 100 μl of LV-SIRT3 and LV-shSIRT3, respectively, at 5×10^8 PFU/ml on the 2nd day after the surgery. The control group received physiological saline, and the vehicle group received SIRT3-shRNA NC lentivirus (LV-Ctrl) under the same conditions. The duration of peri-implant osteolysis induction was 4 weeks.

2.4. Micro-CT analysis

Femurs with Ti rods (n = 6 left femurs from each group) were assessed by high-resolution micro-CT (SkyScan1176, Belgium). Scanning parameters were set as follows: 18 μm per layer under a voltage of 50 kV with a current of 500 μA. A region of interest with a diameter of 1.7 mm, located near the femur growth plate, was chosen for analysis. Three-dimensional (3D) image reconstruction was performed, and morphometric parameters were evaluated, including bone mineral density (BMD), connectivity density (Conn.D), bone volume per total volume (BV/TV), bone surface per bone volume (BS/BV), trabecular number (Tb.N), trabecular thickness (Tb.Th), and trabecular separation (Tb.Sp).

2.5. Biomechanical evaluation

The collected femurs (n = 6 left femurs from each group) were assessed by the biomechanical pull-out test using a material mechanical test system (Zwick, Ulm, Germany). A 3 mm distal resection of the femur metaphysis was performed to expose the Ti rod. Then, the Ti rod was clamped and fixed at the distal part. During the process of tensile loading, the Ti rods were continuously pulled at a velocity of 1 mm per minute along the loading direction. The load of force was recorded to identify the maximum fixation strength.

2.6. Histological, immunohistochemical and immunofluorescence staining

All collected femurs were fixed in 10% formalin for at least 48 h. Parts of the femurs (n = 5 right femurs from each group) were sliced at a thickness of 1 mm under undecalcified conditions. The rest of the femurs were decalcified with 10% ethylenediaminetetraacetic acid (EDTA, Sigma-Aldrich) for 1 month, and Ti rods were carefully removed, embedded and sectioned into 6 μm sections. Routine H&E staining was used to observe the morphological changes in the specimens. Sections were visualized and captured by an LSM510 laser scanning microscope (Carl Zeiss).

Dynamic bone formation was evaluated by using calcein double-labelling staining. All rats were intramuscularly injected with calcein (Sigma-Aldrich) at a dose of 10 mg/kg at 10 days and 2 days before euthanasia. Images of calcein double labelling were visualized by a fluorescence microscope, and parameters including interlabel width, mineralizing surface per bone surface (MS/BS) and mineral apposition rate (MAR) were measured.

Toluidine blue staining was performed to evaluate osseointegration under undecalcified conditions. The sections were immersed in xylene to remove polymethylmethacrylate and gradient hydrated. Then, the cells were rinsed with tap water and stained with 0.05% toluidine blue dye at pH 4. Next, the sections were rinsed with tap water and gradient dehydrated. Finally, the MMA was cleared again with xylene and dried in air. The parameter bone-implant contact (BIC) was measured.

Immunohistochemistry (IHC) staining was used to identify the levels of SIRT3, pyroptosis and pathway-related markers. Briefly, sections were dewaxed and gradient hydrated to retrieve antigen. Then, primary antibodies were added to tissue sections, including SIRT3 (ab189860), pSer9-GSK-3β (ab131097), and NLRP3 (ab214185, all purchased from Abcam, UK), overnight at 4 °C. Next, the sections were blocked with the corresponding secondary antibodies for half an hour. The chromogenic reaction was induced by a DAB Kit (Beyotime, China). Random regions were selected from the entire field of view. IHC-positive cells were measured using Bioquant Osteo 2017 and counted by two independent blinded observers. For statistical accountability, at least 3 different areas were selected in each group to calculate the number of positive cells.

Immunofluorescence staining was performed to detect osteogenesis-related markers. Briefly, tissue sections were dewaxed, antigen-retrieved and blocked with 2% BSA for 60 min. Primary antibodies were then added for incubation overnight at 4 °C, including Runx2 (ab192256) and osterix (ab22552, all from Abcam). After that, the sections were blocked with the corresponding secondary fluorescent antibodies (Alexa Fluor® 647 and 488 (Abcam)) in the dark for 60 min. Next, the nuclei were counterstained with DAPI for 10 min. Finally, the tissue sections were observed with a fluorescence microscope (Zeiss). The intensity of fluorescence was measured using ImageJ.

2.7. Cell culture and osteoblast differentiation

Rat mesenchymal stem cells (rMSCs) were extracted by flushing the tibia and femur of Sprague-Dawley rats with PBS following an established protocol [26] and cultivated in minimum essential alpha medium (α-MEM) supplemented with 10% foetal bovine serum (FBS) and antibiotics (all from Gibco) under 5% CO_2 at 37 °C. For osteogenic differentiation, the medium was α-MEM supplemented with 10% FBS, 0.5 mM vitamin C, 0.1 μM dexamethasone and 10 mM β-glycerophosphate. Osteolysis imitation was induced by adding 10 μg/cm^2 Ti particles, and the medium was replenished every 3 days. The cell seeding density was 1×10^5 cells per well in 6-well plates. In addition, indocyanine green-001 (ICG-001, Selleck), which is a targeted Wnt/β-catenin signalling inhibitor, was applied to pretreat cells to investigate the involved signalling pathways.

2.8. Cell proliferation and viability assay

The cytotoxicity of Ti particles and ICG-001 to rMSCs was evaluated by cell counting Kit-8 (CCK-8; Beyotime) following the manufacturer's protocol. rMSCs were cultured in 96-well plates at a concentration of 5000 cells/well, and various concentrations of Ti particles and ICG-001 were then added and cultivated for 1, 3 and 5 days. After that, the cells were rinsed and incubated with 100 μl of DMEM containing 10 μl of CCK-8 solution for at least 1 h at 37 °C. Finally, the wavelength for measuring absorbance was 450 nm.

2.9. Lentivirus transfection

To overexpress or silence SIRT3, lentivirus vectors that contained the SIRT3 gene were designed (GenePharma, Shanghai, China). The LV-SIRT3 and LV-shSIRT3 carried the green fluorescent protein (GFP) and red fluorescent protein (RFP), respectively. For the silencing of SIRT3, the sequences were as follows: GACTGCTCATCAATCGAGACT. For the overexpression of SIRT3, the targeted sequences were obtained from NCBI Sequence NM_001106313.2. The rMSCs were cultured in plates for 6 h to ensure cell adhesion. Infection of lentiviruses was conducted with a multiplicity of infection (MOI) of 100 when approximately 30% confluence was reached. The infection lasted for 48–72 h before further osteogenic induction. GFP and RFP expression were detected via a fluorescence microscopy (Zeiss). The infectious efficiency was measured using ImageJ. The levels of SIRT3 were identified by qRT-PCR and Western blot analysis.

2.10. Western blot analysis

Proteins in samples were obtained by lysing with radioimmunoprecipitation assay (RIPA; Beyotime) buffer at 4 °C for half an hour, and the supernatant fraction was kept after centrifugation (21,100 × g, 4 °C) for 25 min (Sorvall Legend Micro 21R, Thermo Scientific, Germany). A BCA kit (Sigma) was used to quantify the concentration of protein. Then, proteins (20 μg) were separated by SDS-PAGE (Beyotime) and transferred to a polyvinylidene fluoride membrane (Bio-Rad Laboratories). Next, the membrane was sealed with blocking buffer and incubated in primary antibody solution, including antibodies against SIRT3 (1:1000), Runx2 (1:500), OCN (1:500), osterix (1:500), ALP (1:1000), pSer9-GSK-3β (1:500), total GSK-3β (1:2000), axin-2 (1:1000), β-catenin (1:5000), caspase-1 (1:200), NLRP3 (1:1000), GSDMD (1:1000), IL-1β (1:1000), and IL-18 (1:1000, all obtained from Abcam), overnight at 4 °C. After washing 3 times with Western blot washing solution (Beyotime), the corresponding secondary antibody at a dilution of 1:5000 was added at room temperature for 60 min. Protein bands were captured by enhanced chemiluminescence (ECL; GE Healthcare), and protein quantification was performed using Image Lab 3.0.

2.11. Quantitative real-time PCR assay

Total RNA was isolated from samples using TRIzol reagent (Beyotime), and the density of RNA was quantified using a NanoDrop 2000 spectrophotometer (Thermo Fisher Scientific). Then, complementary DNA (cDNA) was generated from 2 μg of isolated RNA using reverse transcription. Finally, the cDNA was amplified using a reaction system containing 10 μl of qPCRMasterMix (Biotium), 0.5 μl of forward and reverse primer, 2 μl of cDNA, and 7 μl of nuclease-free ddH2O (Invitrogen). Real-time PCR was performed in a CFX96™ thermal cycler (Bio-Rad Laboratories). Each sample assay was performed in triplicate, and the fold change in mRNA expression was determined using the comparative $2^{-\Delta\Delta Cq}$ method. Primers of target genes are listed in Table S1.

2.12. Alkaline phosphatase staining

ALP was assessed as a marker of bone formation. In brief, rMSCs were cultured for 7 days in osteogenic medium. Next, the cells were fixed in 4% paraformaldehyde for half an hour at 4 °C, and then prepared BCIP/NBT (Beyotime) working solution was added to completely cover the cells for incubation in the dark for 30 min. ALP activity was detected by an Alkaline Phosphatase quantification Kit (Jiancheng Bioengineering Institute, Nanjing, China) according to the manufacturer's instructions. Then, ALP activity was assessed at a wavelength of 520 nm (BioTek Instruments, lnc., USA).

2.13. Alizarin red S staining

rMSCs were cultured for 21 days in osteogenic medium. The cells were rinsed and fixed for at least 15 min with 95% ethanol. Next, the cells were dark-incubated with 0.1% ARS staining solution (pH 4.1) for 20 min. Before taking images, the cells were washed 3 times with ddH_2O. A 5% perchloric acid solution was used to dissolve calcium nodules at 37 °C for half an hour, and then the optical density was assessed at 420 nm (BioTek Instruments, lnc., USA).

2.14. Cell immunofluorescence staining

rMSCs were seeded on coverslips with osteogenic differentiation medium in a 24-well plate. Next, the cells were fixed with 4% paraformaldehyde and permeabilized with 0.2% Triton X-100 (Beyotime) for 15 min. Then, coverslips were sealed with blocking buffer for 60 min. Next, the primary antibodies were added for incubation in each well for 12 h at 4 °C, including anti-OCN (1:200). After that, the cells were rinsed, and the corresponding secondary fluorescent antibody (either Alexa Fluor® 488 or 647 (Abcam)) was added for incubation in the dark for 60 min. Fluorescently stained cells were then counterstained with DAPI for 10 min. Coverslips were placed on microscope slides with fluorescence anti-fade solution (Beyotime) and observed with a fluorescence microscope (Zeiss). The intensity of fluorescence was measured using ImageJ.

2.15. Determination of IL-1β and IL-18 secretion

After culturing rMSCs with different interventions, the medium was collected for enzyme-linked immunosorbent assays (ELISAs). The levels of IL-1β and IL-18 secretion in the culture supernatant were measured separately using different ELISA kits (R&D Systems, USA) in accordance with the manufacturer's instructions.

2.16. Statistical analysis

Values are represented as the means ± standard deviation. Student's t-test was performed to determine the significance of differences between two groups, and one-way ANOVA followed by Tukey's test was used to determine multiple comparisons. SSPS 25.0 was used for statistical analysis. Statistical significance was defined as $p < 0.05$.

3. Results

3.1. Effect of SIRT3 on amelioration of periprosthetic osteolysis by promoting osteogenesis in vivo

To investigate the efficacy of SIRT3 in wear particle-induced periprosthetic bone loss, we first collected the removed clinical tissues from patients who suffered from osteoarthritis (OA) who underwent primary

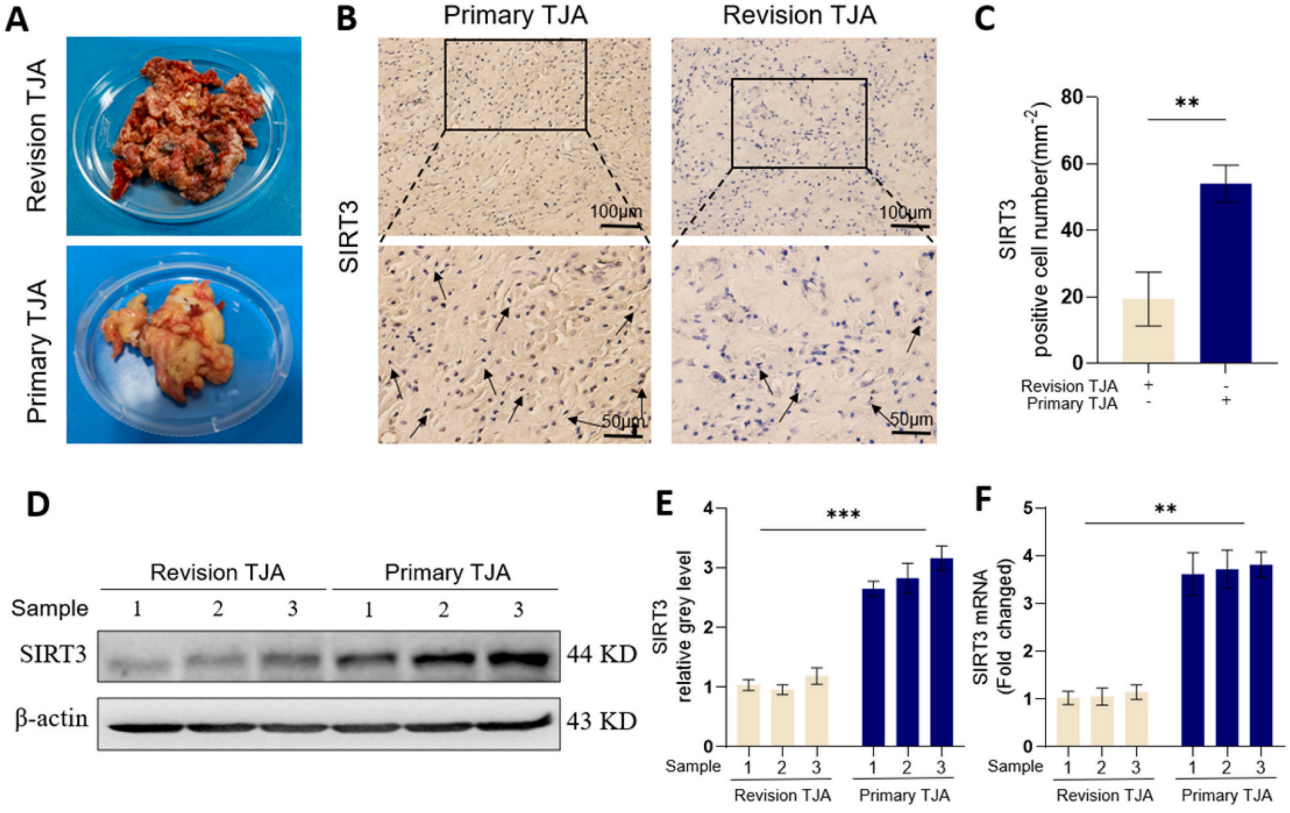

Fig. 1. The expression of SIRT3 in primary TJA and revision TJA tissues. (A) Images of clinical tissues collected from primary TJA and revision TJA. (B) Representative images of IHC staining of the expression of SIRT3. (C) Semiquantitative analysis of SIRT3-positive cells, at least 3 different areas were selected in each group for calculating the number of positive cells. (D-E) Protein levels of SIRT3 in primary TJA and revision TJA samples. (F) mRNA levels of SIRT3 in primary TJA and revision TJA samples. (n = 3 per group. Values are shown as the means ± s.d. $^{**}p < 0.01$ and $^{***}p < 0.005$).

total joint arthroplasty (TJA) and those who suffered from aseptic loosening who underwent revision TJA (Fig. 1A). Immunohistochemical staining revealed that SIRT3 expression in revision TJA tissues was significantly decreased relative to that in primary TJA tissues (Fig. 1B and C). Moreover, Western blot and quantitative analysis (Fig. 1D–E) demonstrated that the protein levels of SIRT3 were significantly higher in primary TJA tissues than in revision TJA tissues. Furthermore, the qRT-PCR analysis (Fig. 1F) was consistent with the Western blot results. These results suggest that SIRT3 may be related to wear particle-induced periprosthetic osteolysis.

Next, a Ti particle-stimulated periprosthetic osteolysis rat model was used to further explore the effect of SIRT3 in PPO *in vivo*. The expression of SIRT3 was regulated through lentivirus injection, and feasibility was identified by Western blot (Fig. S1). Additionally, lentivirus toxicity on organs was not observed *in vivo* (Fig. S2). As shown in the micro-CT and 3D reconstruction images (Fig. 2A), the periprosthetic bone mass was significantly damaged in the vehicle group and rescued by treatment with LV-SIRT3. Meanwhile, the bone mass was further destroyed by the interference of LV-shSIRT3. In addition, the quantitative analysis of bone parameters (Fig. 2B–H) showed that the BMD, BV/TV, Tb.N, Tb.Th and Conn.D values decreased significantly and the BS/BV and Tb.Sp values increased dramatically in the vehicle group compared with the control group. Bone loss was alleviated significantly when treated with LV-SIRT3. The BMD, BV/TV, Tb.N, Tb.Th and Conn.D values in the LV-shSIRT3 group was significantly lower than those in the LV-SIRT3 group. Moreover, the maximum fixation strength of the Ti rods dramatically increased in the LV-SIRT3 group (Fig. 2I). A decrease in the maximum fixation strength was also observed in LV-shSIRT3. These data showed that the periprosthetic bone mass was preserved by upregulating the expression of SIRT3.

Consistently, H&E and toluidine blue staining (Fig. 3A and B) confirmed the suppression of periprosthetic osteolysis by treatment with LV-SIRT3. Semiquantitative analysis of H&E staining (Fig. 3E) and toluidine blue staining (Fig. 3F) demonstrated that SIRT3 treatment significantly increased the mineral surface of bone and protected the trabeculae around prostheses. Calcein double labelling (Fig. 3C & G-H) showed that SIRT3 treatment increased the distance between the double labels compared with the vehicle group, and the mineralizing surface/bone surface and mineral apposition rate were enhanced in the LV-SIRT3 group compared with the vehicle group. Furthermore, immunofluorescence staining was performed to evaluate the ability of SIRT3 to enhance osteogenesis during the process of periprosthetic bone loss. The expression of the osteogenic markers Runx2 and osterix (Fig. 3D) was upregulated in the LV-SIRT3 group and inhibited in the LV-shSIRT3 group, which demonstrated that Ti particles suppressed the expression of osteogenic markers during periprosthetic osteolysis, but SIRT3 intervention rescued bone formation. Collectively, these results indicated that Ti particle-stimulated periprosthetic osteolysis was alleviated by enhancing osteogenesis via targeted regulation of SIRT3 *in vivo*.

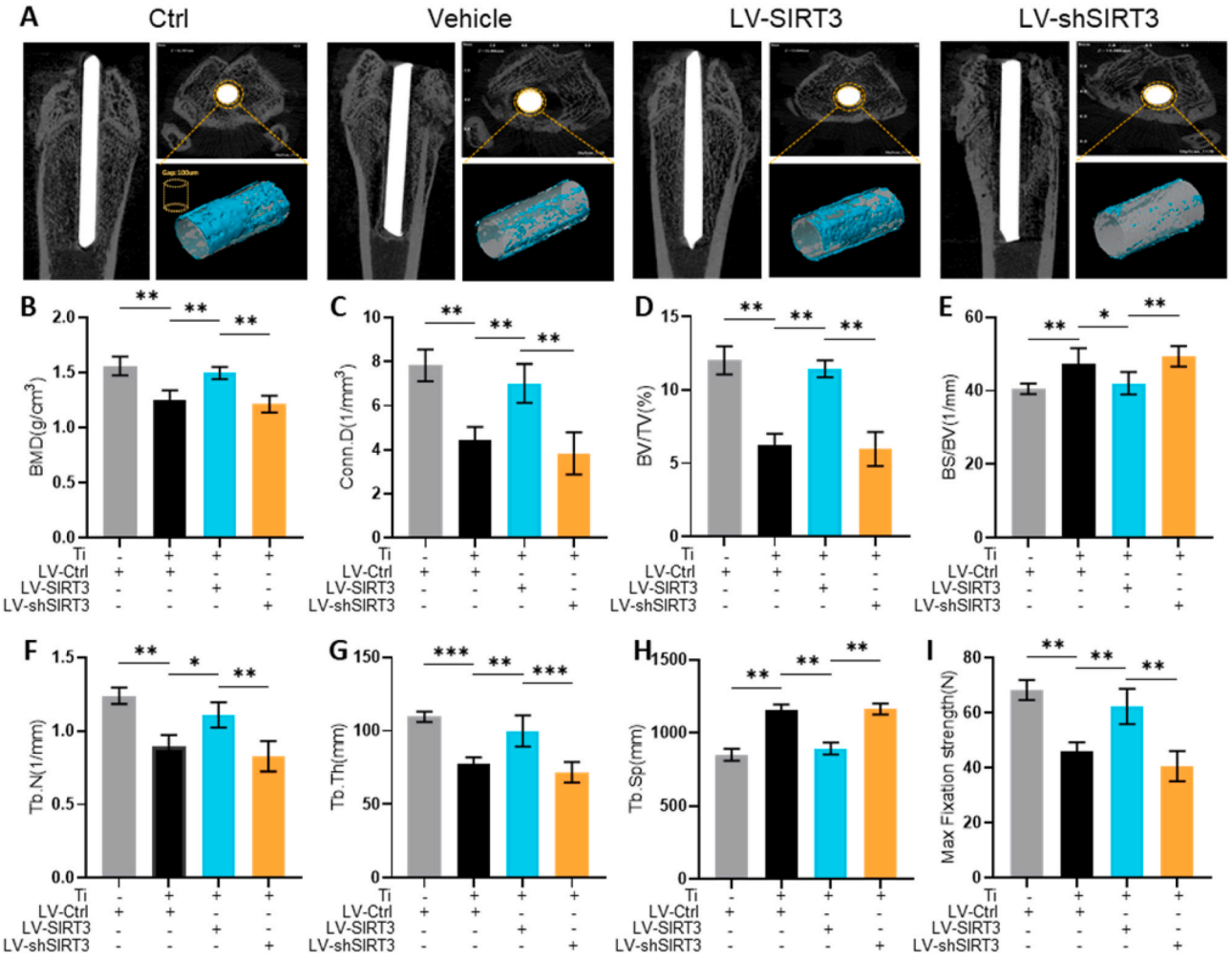

Fig. 2. SIRT3 treatment moderated Ti particle-induced bone destruction and enhanced bone formation in a periprosthetic osteolysis rat model. (A) Representative images of Micro-CT. (B) BMD (mg/mm^3). (C) Conn.D (mm^{-3}). (D) BV/TV (%). (E) BS/BV (mm^{-1}). (F) Tb.N (mm^{-1}). (G) Tb.Th (mm). (H) Tb.Sp (mm). (I) Max fixation strength (N) identified by biomechanical evaluation. (n = 6 per group. Values are shown as the means ± s.d. *$p < 0.05$ and **$p < 0.01$).

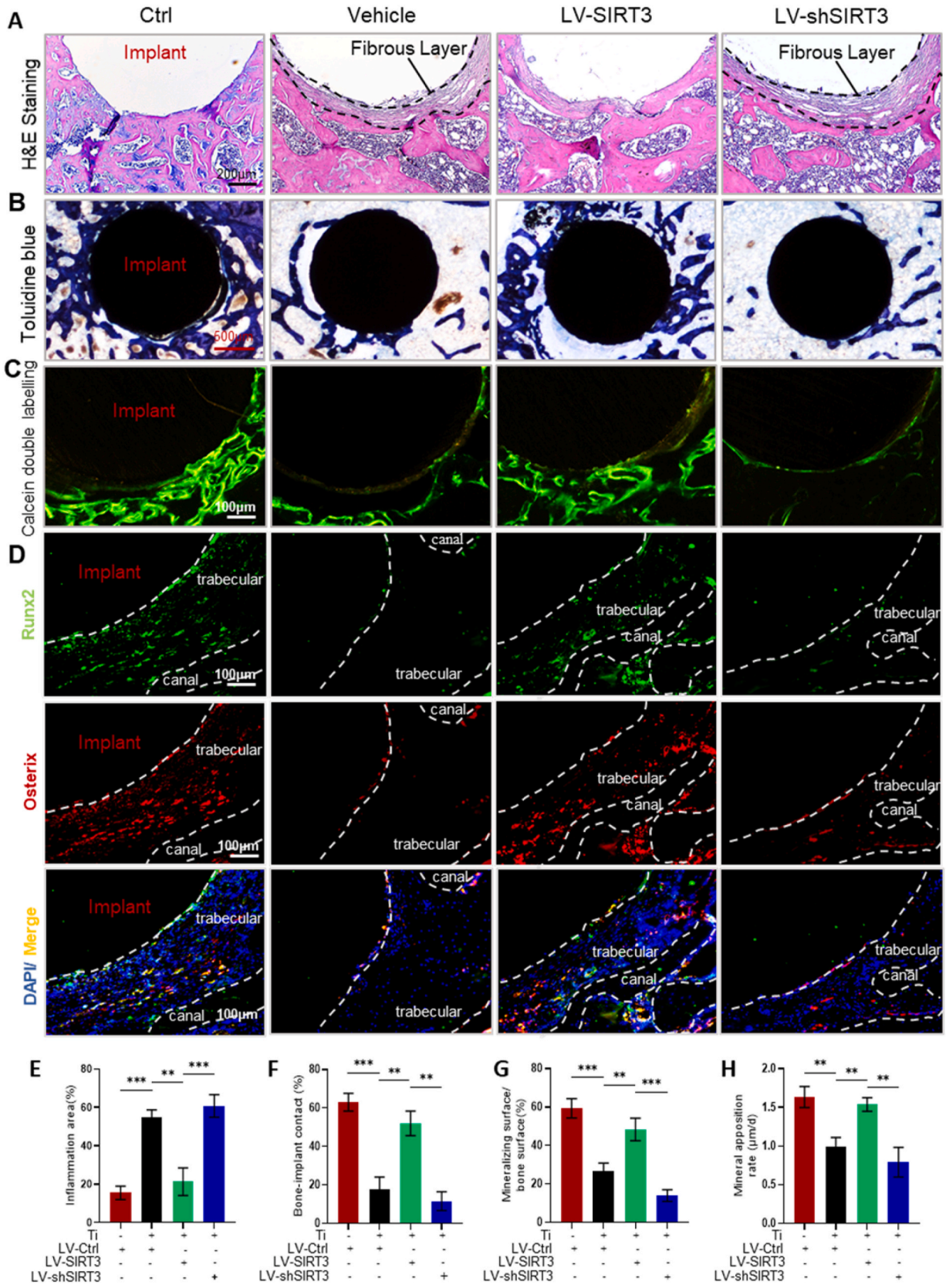

Fig. 3. SIRT3 treatment alleviated Ti particle-induced PPO in histological sections of distal femurs. (A) Representative images of H&E staining. (B) Representative images of toluidine blue staining. (C) Representative images of calcein double-labelling staining. (D) Representative images of immunofluorescence, red (osterix), green (Runx2), and blue (nuclei). (E) Inflammatory areas identified with black dotted lines showing the fibrous layer, n = 6 per group. (F) Bone-implant contact (BIC, %), n = 5 per group. (G) Mineralizing surface/bone surface (%), n = 5 per group. (H) Mineral apposition rate (μm/day), n = 5 per group. (Values are shown as the means ± s.d. $^{**}p < 0.01$ and $^{***}p < 0.005$).

3.2. Effect of SIRT3 on amelioration of osteogenic reduction induced by Ti particles in vitro

To gain insight into the efficacy of SIRT3 on bone formation in the presence of Ti particles *in vitro*, we used lentivirus transfection to regulate the expression levels of SIRT3. The lentivirus infectious efficiency in cells was detected via fluorescence microscopy (Fig. S3). Western blot analysis revealed the feasibility of upregulating and silencing the expression of SIRT3 via LV-SIRT3 and LV-shSIRT3, respectively (Figs. S4A and B). Consistently, the qRT-PCR results (Fig. S4G) also verified the effectiveness of the lentivirus. Meanwhile, we found that osteogenic differentiation was activated by overexpression of SIRT3 and inhibited when SIRT3 expression was knocked down without Ti particle intervention (Fig. S4A & C-K).

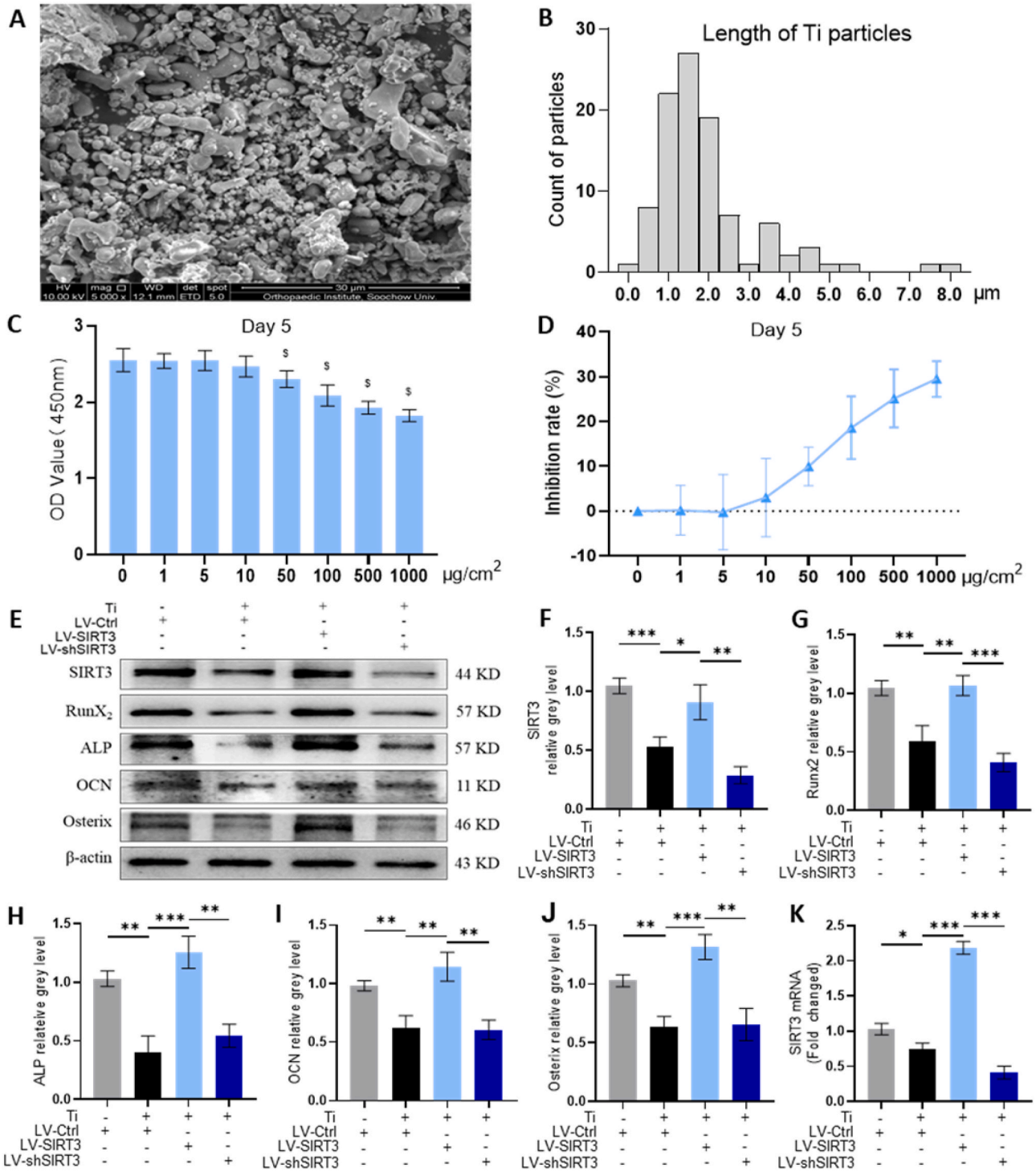

Fig. 4. SIRT3 treatment ameliorated Ti particle-induced suppression of osteogenic differentiation in rMSCs. (A) Scanning electron microscopy (SEM) image of Ti particles. (B) Distribution of Ti particles size. (C) Cell viability after incubation for 5 days with different concentrations of Ti particles was assessed using a CCK-8 kit. $\$p < 0.05$, compared with basal group. (D) Rate of inhibition rate on rMSCs. (E-J) Protein levels of SIRT3, Runx2, ALP, OCN and osterix. The cells were incubated in the presence of 10 μg/cm^2 of Ti particles. (K) mRNA levels of SIRT3. (n = 3 per group. The cell seeding density was 1×10^5 cells per well in 6-well plates. Values are shown as the means ± s.d. $^*p < 0.05$, $^{**}p < 0.01$ and $^{***}p < 0.005$).

The Ti particles that we used in this study were observed under scanning electron microscopy (SEM, Fig. 4A), and the length of the Ti particles was measured; over 90% had diameters less than 4 μm (Fig. 4B). Moreover, the results of CCK8 analysis determined that the viability of cells was unaffected below the concentration of 10 μg/cm^2 Ti particles over 1, 3 and 5 days (Fig. 4C and D, Figs. S5A and B). Hence, rMSCs were stimulated with 10 μg/cm^2 Ti particles after lentivirus interference. Western blot and quantitative analysis (Fig. 4E–J) demonstrated that the protein levels of osteogenic markers were significantly upregulated by LV-SIRT3 treatment compared with vehicle treatment, which indicated that upregulation of SIRT3 expression alleviated Ti particle-induced osteogenic reduction. In contrast, the rescued effect on osteogenic reduction vanished when SIRT3 was silenced. Furthermore, the qRT-PCR analysis (Fig. S5C) was also consistent with the Western blot results.

Additionally, immunofluorescence staining (Fig. 5A) indicated that OCN expression, which is located on the plasma membrane, was increased by targeted upregulation of SIRT3 expression. The fluorescence intensity was further decreased by treatment with LV-shSIRT3 (Fig. 5D). ALP staining (Fig. 5B and E) showed that treatment with LV-SIRT3 moderated the inhibition of Ti particle-induced osteogenic differentiation of rMSCs. Moreover, Alizarin red S staining (ARS, Fig. 5C) confirmed the rescued effect of SIRT3 on bone formation in the presence of Ti particles, and the semiquantitative analysis of ARS (Fig. 5F) indicated that the mineralization of cells was greatly accelerated by approximately 385.9% in the LV-SIRT3 group relative to the group treated with Ti particles only. Overall, these data further confirmed the ability of SIRT3 to rescue reduced osteogenic differentiation induced by Ti particles in rMSCs.

3.3. *Effect of SIRT3 on pyroptosis-related NLRP3 inflammasome inhibition in vivo and in vitro*

To evaluate whether SIRT3 regulated pyroptosis-associated NLRP3 inflammasome activation during the process of Ti particle-induced prosthetic osteolysis, we first assessed NLRP3 inflammasome expression in collected femurs. Immunohistochemistry staining (IHC, Fig. 6A) revealed that LV-SIRT3 treatment significantly decreased NLRP3 expression relative to vehicle treatment, whereas LV-shSIRT3 intervention further upregulated NLRP3 activation. The semiquantitative analysis of IHC staining (Fig. 6C) indicated that many NLRP3-positive cells infiltrated around the prosthesis in the vehicle group; in contrast, few NLRP3-positive cells were observed after targeting upregulated SIRT3 expression. Furthermore, we found that the expression of pyroptosis-associated proteins was dramatically increased by stimulation of Ti particles in rMSCs, and downstream proinflammatory cytokines were promoted by the NLRP3 inflammasome in cells treated with Ti particles only (Fig. 6B). However, the interference of LV-SIRT3 suppressed the activation and expression of the NLRP3 inflammasome as well as downstream factors. Quantitative assessment by western blotting (Fig. 6D–J) also verified that pyroptosis-related proteins were decreased by targeted upregulation of SIRT3 expression. Consistent with the

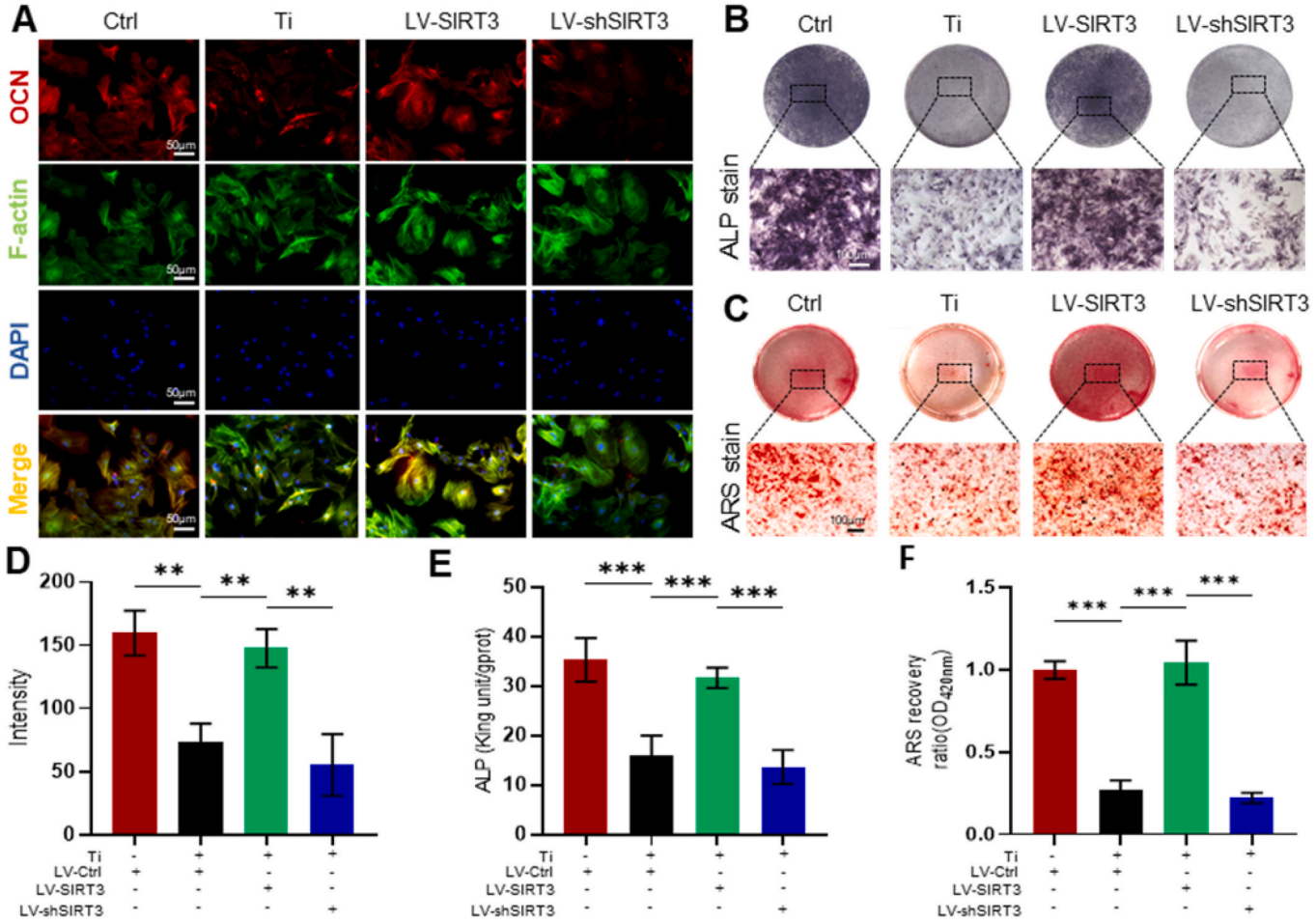

Fig. 5. SIRT3 treatment mitigated Ti particle-induced suppression of osteogenesis and mineralization in rMSCs. (A) Representative images of immunofluorescence staining; red (OCN), green (Phalloidin), and blue (nuclei). (B) Representative images of ALP staining at 7 days. (C) Representative images of ARS staining at 21 days. (D) Semiquantitative evaluation of fluorescence intensity. (E) Quantitative evaluation of ALP activity. (F) Semiquantitative evaluation of the ARS recovery ratio. (n = 6 per group. The cell seeding density was 5 × 10^3 cells per well in 24-well plates. Values are shown as the means ± s.d. $^{**}p < 0.01$ and $^{***}p < 0.005$).

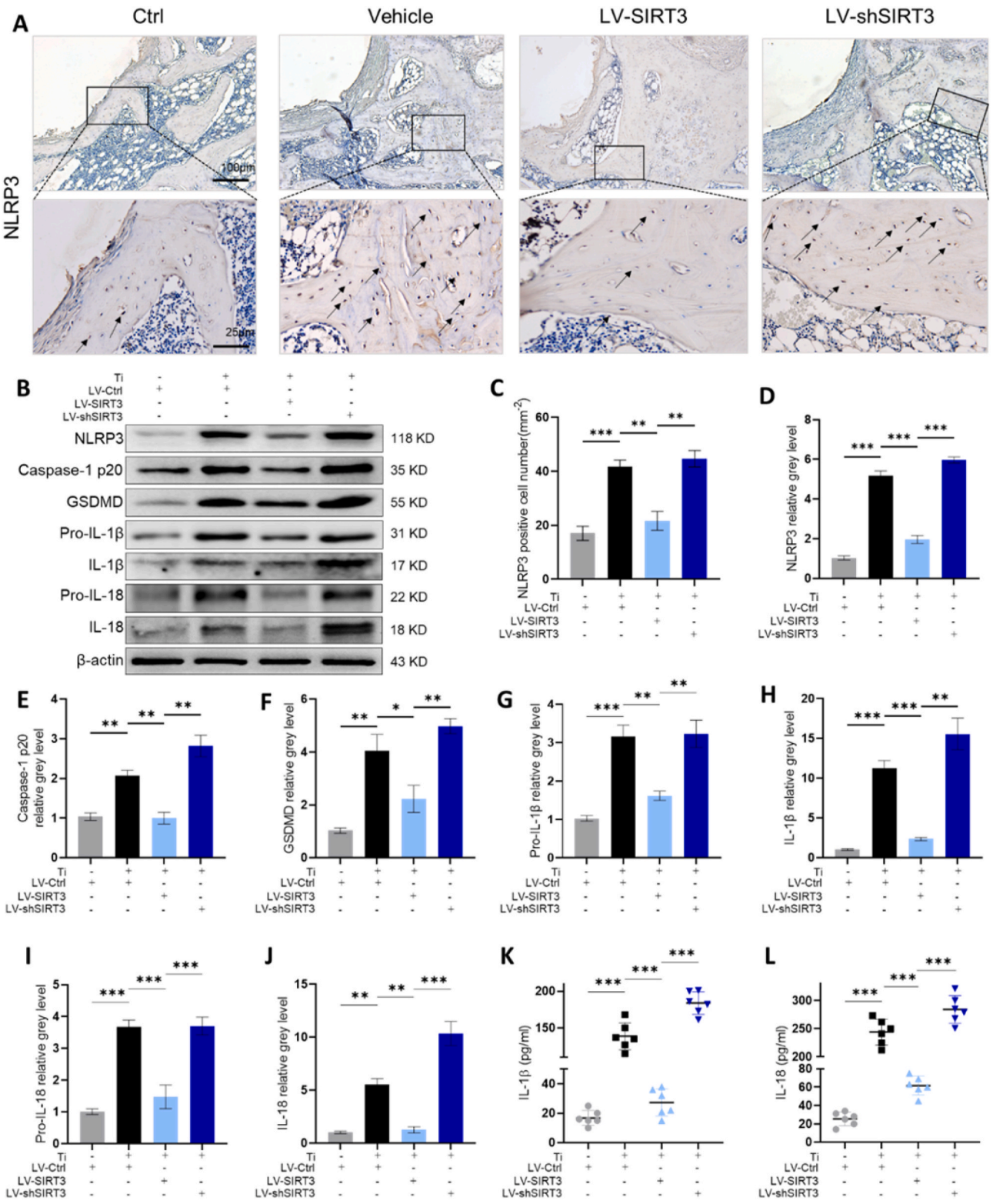

Fig. 6. SIRT3 treatment suppressed Ti particle-stimulated activation of the pyroptosis-related NLRP3 inflammasome. (A) Representative images of IHC staining, identified with black arrows showing NLRP3-positive cells. (B) Western blot of pyroptosis-related proteins. (C) Semiquantitative evaluation of NLRP3-positive cells (n = 6 per group). (D-J) Protein levels of NLRP3, caspase-1, GSDMD, IL-1β, and IL-18, n = 3 per group. (K-L) Secretion of IL-1β and IL-18 in the culture medium, n = 6 per group. (The cell seeding density was 1×10^5 cells per well in 6-well plates. Values are shown as the means ± s.d. $*p < 0.05$, $**p < 0.01$ and $***p < 0.005$).

Western blot results, the qRT-PCR results (Fig. S6) showed an observable effect in which LV-SIRT3 reduced the mRNA levels of NLRP3, caspase-1, GSDMD, IL-1β and IL-18. To determine the secreted levels of IL-1β and IL-18, ELISAs were performed. The secretion of IL-1β and IL-18 was inhibited by treatment with LV-SIRT3, while treatment with LV-shSIRT3 enhanced the secretion of these cytokines (Fig. 6K-L). Consequently, SIRT3 exhibited an inhibitory role in pyroptosis-related NLRP3 inflammasome activation stimulated by Ti particles *in vivo* and *in vitro*.

3.4. The effect of SIRT3 on the alleviation of Ti particle-induced PPO relied on the GSK-3β/β-catenin signalling pathway

To explore the possible mechanisms by which SIRT3 treatment attenuated Ti particle-induced osteogenic reduction and inhibited activation of the NLRP3 inflammasome in periprosthetic osteolysis, we assessed the pivotal markers involved in the corresponding signalling pathways. Western blot analysis (Fig. 7A) indicated that the protein levels of pSer9-GSK-3β, axin-2 and β-catenin were decreased in cells stimulated with Ti particles, while the targeted upregulation of SIRT3 significantly reversed the expression of these proteins. Quantitative Western blot analysis (Fig. 7B–D) indicated that the pSer9-GSK-3β to GSK-3β ratio and the levels of β-catenin and axin-2 were significantly elevated in the LV-SIRT3 group compared with the vehicle group. Consistently, the qRT-PCR results (Fig. S7) also confirmed that the mRNA levels of axin-2 and β-catenin were much higher in the LV-SIRT3 group than in the vehicle group. These data illustrated that the GSK-3β/β-catenin pathway might be involved in Ti particle-induced periprosthetic osteolysis mediated by SIRT3. IHC staining was performed in collected femurs to further verify whether regulation of SIRT3 inhibited wear particle-induced periprosthetic osteolysis through GSK-3β/β-catenin signalling. These results (Fig. 7E) revealed that pSer9-GSK-3β expression was elevated by LV-SIRT3 treatment. Moreover, the semiquantitative analysis of IHC staining (Fig. 7F) showed that few pSer9-GSK-3β-positive cells were identified in the group stimulated with Ti particles, while numerous IHC-positive cells were identified under SIRT3 intervention. Overall, these results suggested that upregulation of SIRT3 levels impaired Ti particle-induced periprosthetic osteolysis relying on GSK-3β/β-catenin signalling.

To further verify whether the protective effect of SIRT3 on Ti particle-induced PPO was dependent on GSK-3β/β-catenin signalling, indocyanine green-001 (ICG-001), which is a targeted Wnt/β-catenin signalling inhibitor, was applied to pretreat cells. The cytotoxicity of ICG-001 on cells was measured first using a CCK-8 kit (Fig. 8A and B), and a concentration of 10 μM ICG-001 was selected to treat cells with 10 μg/cm^2 Ti particles and LV-SIRT3. Western blot results (Fig. 8C–G) showed that the expression of osteogenic markers was dramatically decreased by the administration of ICG-001. Consistently, qRT-PCR (Fig. S8) revealed that the mRNA levels of osteogenesis-related markers were lower in the ICG-001 treatment group than in the LV-SIRT3 group. In addition, ARS staining and ALP staining (Fig. 8H and I) further verified the inhibitory effects of ICG-001 on bone formation and mineralization, which indicated that ICG-001 blocked the beneficial effects of SIRT3 in Ti particle-induced osteogenic reduction.

Moreover, the protein and mRNA levels of pyroptosis-related markers were significantly increased in the LV-SIRT3+ICG-001 group relative to the LV-SIRT3 group (Fig. 9A and B, Fig. S9A). Additionally, the Western blot (Fig. 9C and D) and qRT-PCR (Fig. S9B) results indicated that ICG-001 treatment decreased the mRNA and protein levels of pSer9-GSK-3β, axin-2 and β-catenin relative to the LV-SIRT3 group. Collectively, these data illustrated that upregulation of SIRT3 reversed Ti particle-induced GSK-3β/β-catenin signalling inhibition.

4. Discussion

Periprosthetic osteolysis is an almost unavoidable issue, followed by total joint arthroplasty, which leads to progressive bone mass loss stimulated by wear particles [27]. Several cells, including macrophages, lymphocytes, fibroblasts, osteoclasts and osteoblasts, are correlated with the development of wear particle-induced periprosthetic osteolysis, which breaks bone homeostasis between bone resorption and formation [28]. Previous studies have suggested that inhibition of bone regeneration dominates in the initiation of PPO [7,29]. Moreover, downregulation of bone resorption by traditional anti-osteoporosis drugs can attenuate the damage to the structural bone matrix, whereas the quantity of bone cannot be reversed and repaired. Therefore, ameliorating the wear particle-induced inhibition of osteogenic differentiation might be a key factor for PPO therapy.

SIRT3, an NAD^+-dependent deacetylase of mitochondria, regulates the function of mitochondria in diverse activities, including energy metabolism [30,31], oxidative stress [14], apoptosis [32], ageing [33] and cancer progression [34]. Moreover, some findings have revealed

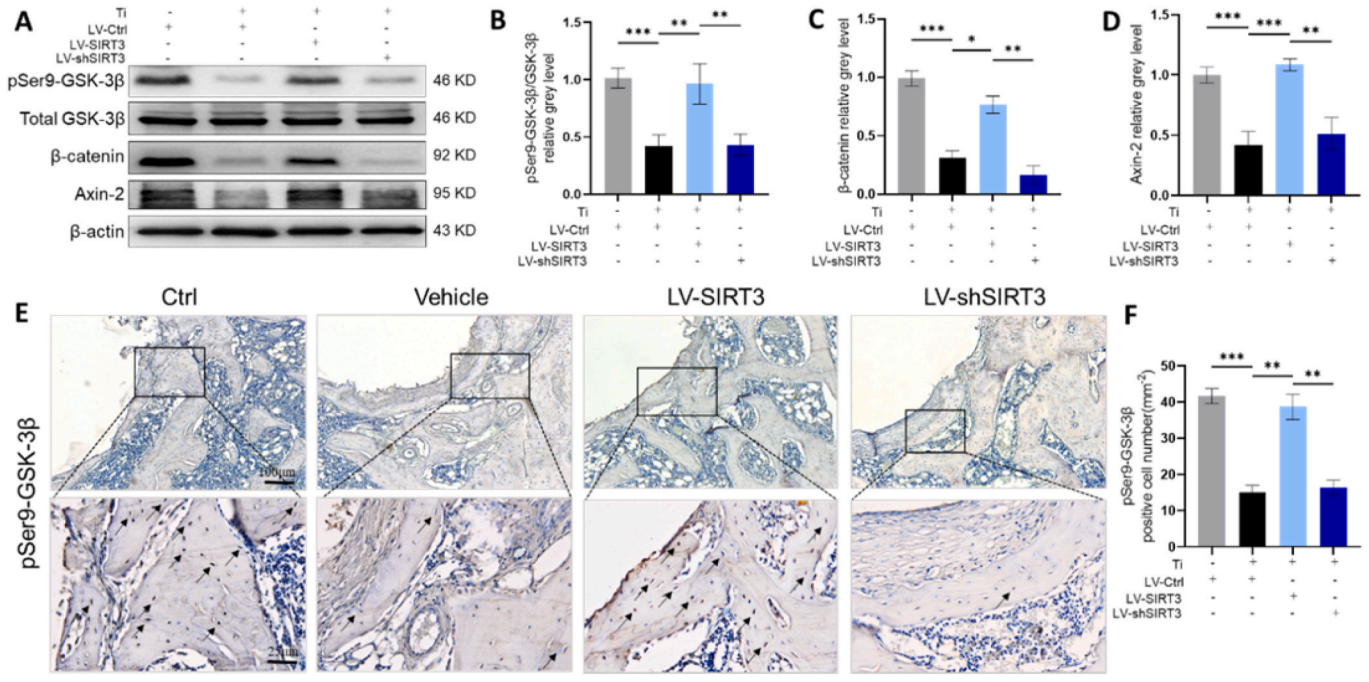

Fig. 7. SIRT3 mediated GSK-3β/β-catenin signalling *in vitro* and *in vivo*. (A-D) Protein levels of pSer9-GSK-3β/total GSK-3β, axin-2 and β-catenin, n = 3 per group. (E) Representative images of IHC staining of phosphorylation of Ser9-GSK-3β, identified with black arrows showing the IHC-positive cells, n = 6 per group. (F) Semiquantitative analysis of pSer9-GSK-3β-positive cells. (The cell seeding density was 1 × 10^5 cells per well in 6-well plates. Values are shown as the means ± s.d. $^*p < 0.05$, $^{**}p < 0.01$ and $^{***}p < 0.005$).

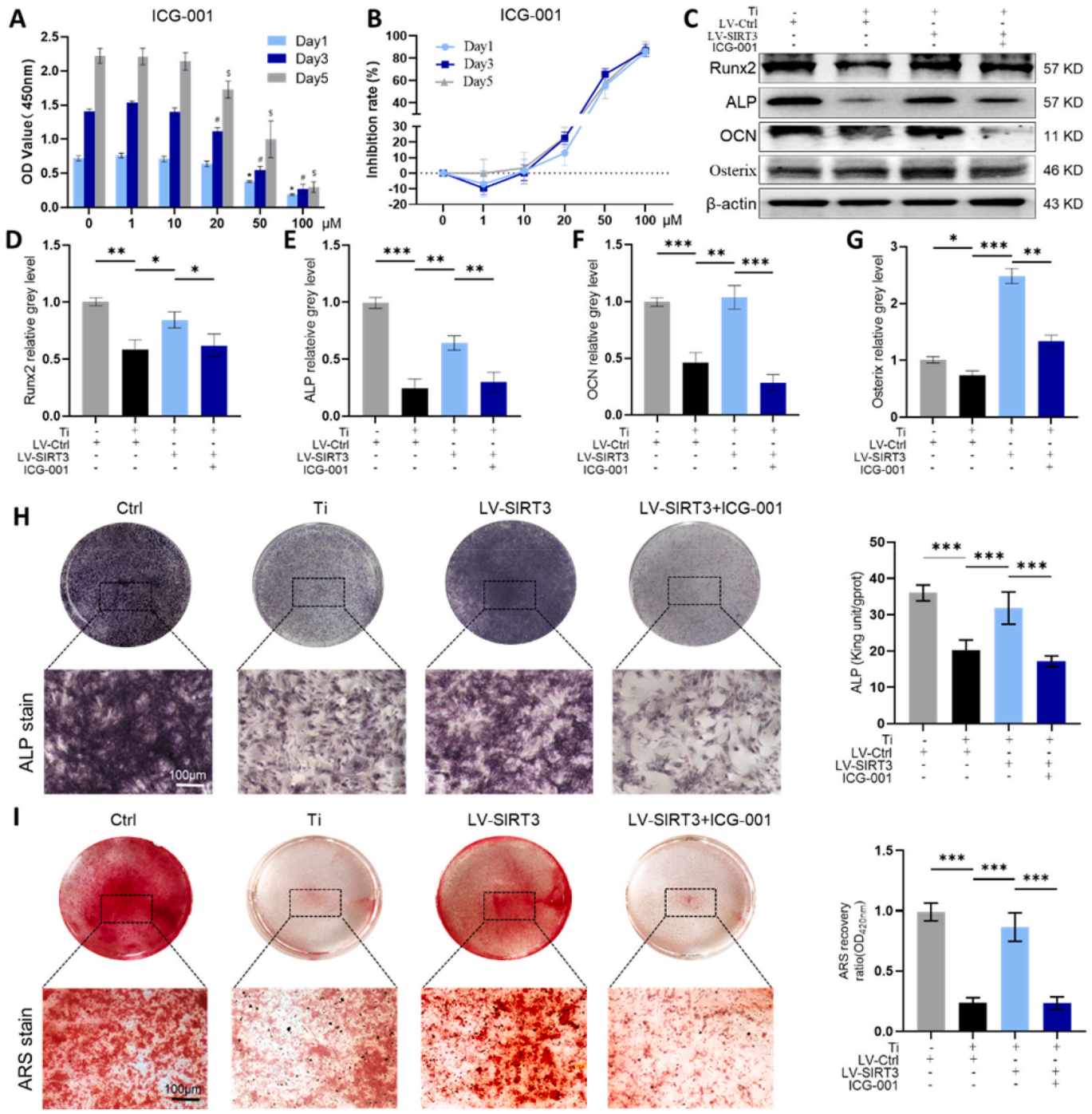

Fig. 8. ICG-001 reduced the efficacy of SIRT3 on bone formation and mineralization in rMSCs. (A) Cell viability after incubation for 1, 3, or 5 days was assessed by a CCK-8 kit. *$p < 0.05$, compared with the basal group (day 1), #$p < 0.05$, compared with the basal group (day 3), and \$$p < 0.05$, compared with the basal group (day 5). (B) Rate of inhibition on rMSCs. (C-G) Expression levels of osteogenic-related proteins, n = 3 per group. (H) ALP staining and quantitative evaluation of ALP activity, n = 6 per group. (I) ARS staining and semiquantitative evaluation of the ARS recovery ratio, n = 6 per group. (The cell seeding density was 1×10^5 cells per well in 6-well plates and 5×10^3 cells per well in 24-well plates. Values are shown as the means ± sd. *$p < 0.05$, **$p < 0.01$ and ***$p < 0.005$).

that SIRT3 might be a positive factor in bone remodelling [16–18]. However, whether SIRT3 attenuates wear debris-stimulated PPO has not been reported. Interestingly, we first found that SIRT3 was significantly lower expressed in clinical samples from patients underwent revision TJA compared to those from primary TJA. The different levels of SIRT3 in revision and primary TJA tissues suggested a critical role for SIRT3 in regulating the wear particle-induced periprosthetic osteolysis. Similar modulation of SIRT3 was implicated in previous studies that SIRT3 expression was inhibited in acute lung injury, acute kidney injury, cardiac hypertrophy, etc [35–37]. Based on this, we speculated that regulation of SIRT3 would alleviate PPO. So, we used lentivirus to selectively regulate the SIRT3 expression, observing that upregulated SIRT3 reversed Ti particle-induced osteogenic reduction *in vitro* and ameliorated periprosthetic osteolysis by promoting osteogenesis *in vivo*. Moreover, for the first time, we showed that overexpression of SIRT3 alleviated Ti particle-induced PPO via NLRP3 inflammasome inhibition and osteogenesis enhancement.

A relationship between SIRT3 and inflammasomes has been found in

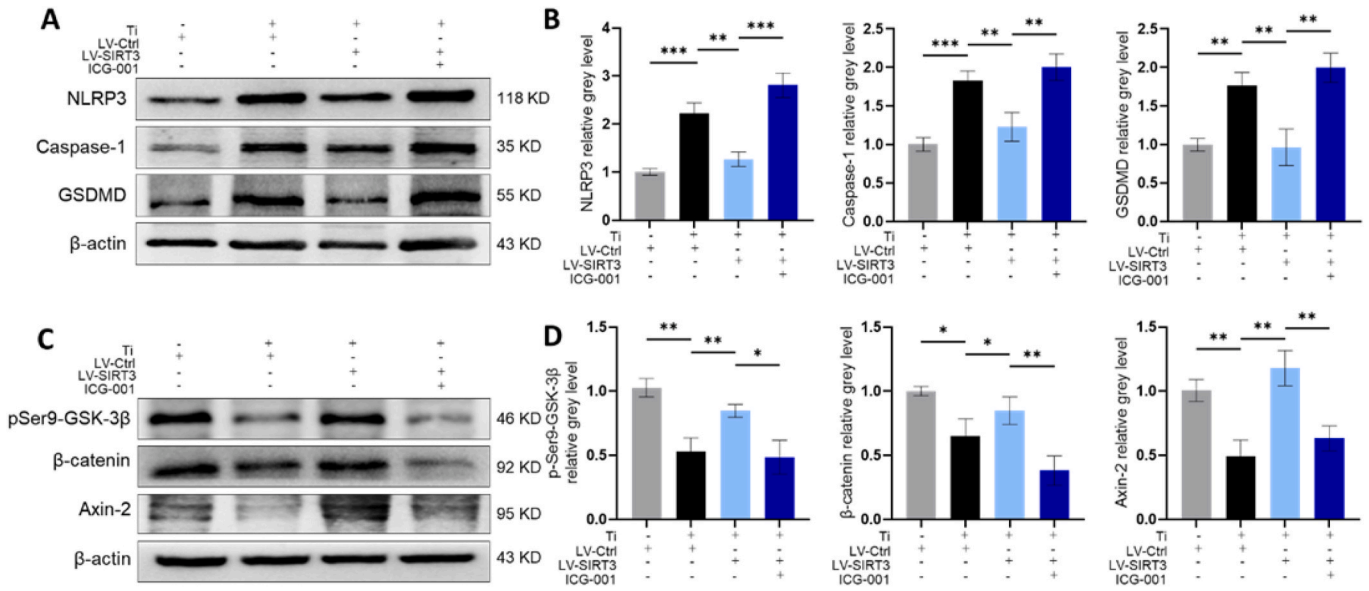

Fig. 9. ICG-001 reversed the inhibitory effect of SIRT3 on the NLRP3 inflammasome and β-catenin in rMSCs. (A-B) Protein levels of NLRP3, caspase-1, and GSDMD. (C-D) Protein levels of pSer9-GSK-3β, axin-2 and β-catenin. (n = 3 per group. The cell seeding density was 1×10^5 cells per well in 6-well plates. Values are shown as the means ± sd. $^*p < 0.05$, $^{**}p < 0.01$ and $^{***}p < 0.005$).

several diseases, suggesting that the assembly and activation of the NLRP3 inflammasome are blunted by SIRT3 [24]. Zhao et al. showed that SIRT3 moderated acute kidney injury by downregulating the NLRP3 inflammasome, suppressing oxidative stress and decreasing IL-18 and IL-1β [36]. Zheng et al. revealed that SIRT3 protects against neurodamage in hyperglycaemic intracerebral haemorrhage by decreasing NLRP3 levels through SOD2 deacetylation and ROS scavenging [38]. Consistently, the results of our study showed that SIRT3 ameliorated wear particle-induced PPO by suppressing the NLRP3 inflammasome and the downstream component caspase-1, thereby blocking the inflammatory cascade, including IL-18 and IL-1β.

Growing evidence has illustrated that the NLRP3 inflammasome is activated by prosthetic particles and likely participates in prosthetic loosening [22,39]. McCall et al. demonstrated that osteoblasts express the NLRP3 inflammasome in bacteria-induced cell death and contribute to bone loss [40]. Wang et al. revealed that promotion of the NLRP3 inflammasome in BMSCs could suppress osteogenic differentiation [41]. Similarly, the results of our study revealed that bone formation-related markers were significantly decreased in the NLRP3 inflammasome activation group, while downregulation of the NLRP3 inflammasome reversed the effect of osteogenesis inhibition. Collectively, these results revealed that wear particle-induced inhibition of osteogenic differentiation was attenuated by decreased NLRP3 inflammasome activity in PPO.

Previous research has suggested that Wnt/β-catenin signalling is a crucial regulator of the proliferation and differentiation of osteoblasts to promote osteogenesis [42–44]. Meanwhile, GSK-3β, known as a serine/threonine protein kinase, can inactivate and degrade β-catenin to inhibit bone formation [45]. In our study, Ti particles decreased the level of β-catenin as well as its downstream gene axin-2; however, upregulated SIRT3 reversed the expression of axin-2 and β-catenin. The pSer9-GSK-3β to GSK-3β fraction was elevated by overexpression of SIRT3. Taken together, SIRT3 upregulated the levels of axin-2 and β-catenin and interfered with GSK-3β by phosphorylating at Ser9.

To further verify whether SIRT3 alleviated PPO by activating GSK-3β/β-catenin signalling, ICG-001, a targeted Wnt/β-catenin signalling pathway inhibitor, was applied to coculture. Our study showed that osteoblastic differentiation and bone formation were reduced, while the expression of the NLRP3 inflammasome was increased with ICG-001 administration. In addition, ICG-001 treatment alleviated the SIRT3-mediated rescue effect on the Ti particle-induced suppression of GSK-3β/β-catenin signalling. Collectively, these data revealed that SIRT3 protected Ti particle-induced inhibition of osteogenesis and suppressed the NLRP3 inflammasome in PPO through GSK-3β/β-catenin signalling.

There were still some limitations. In this study, we used Ti particles to trigger osteolysis on account of their stabilized and easily adherent features [46]. In the clinic, ultrahigh molecular weight polyethylene (UHMWPE) debris, rather than sterile Ti particles, is the major trigger for PPO. Thus, the effect of SIRT3 on the UHMWPE osteolysis model should be further explored. However, Ti and UHMWPE particles could comparably trigger periprosthetic osteolysis, and UHMWPE particles easily floated in cell culture. Moreover, we regulated the expression of SIRT3 by intramuscular injection of lentivirus, which was identified as a simple and effective way to evaluate the effect of SIRT3 on periprosthetic osteolysis and NLRP3 inflammasome, also explored the possible involved signalling pathways. However, it is not easy to applied in clinical trials. In future, we would attempt to do some surface modifications of the titanium bars to achieve these effects for better clinical application. In addition, osteoclastic resorption and inflammation are two other key factors in wear particle-induced PPO. Some studies have demonstrated the regulatory role of SIRT3 in inflammation and osteoclastic resorption [16,47]. It would be essential to explore the potential role of SIRT3 in ameliorating inflammation and osteoclastogenesis in PPO. Finally, except for the GSK-3β/β-catenin signalling pathway, other signalling pathways subverted in PPO cannot be ignored and are worth further exploration.

5. Conclusion

Comprehensively, our study indicated that SIRT3 exerts protective effects on Ti particle-induced periprosthetic osteolysis by mitigating osteogenic reduction and that inhibiting the NLRP3 inflammasome relies on the promotion of the GSK-3β/β-catenin signalling pathway (Scheme 1). These findings may indicate a rational new treatment against wear debris-induced PPO by deacetylase-dependent inflammasome attenuation.

CRediT authorship contribution statement

Kai Zheng: Conceptualization, Methodology, Writing – original

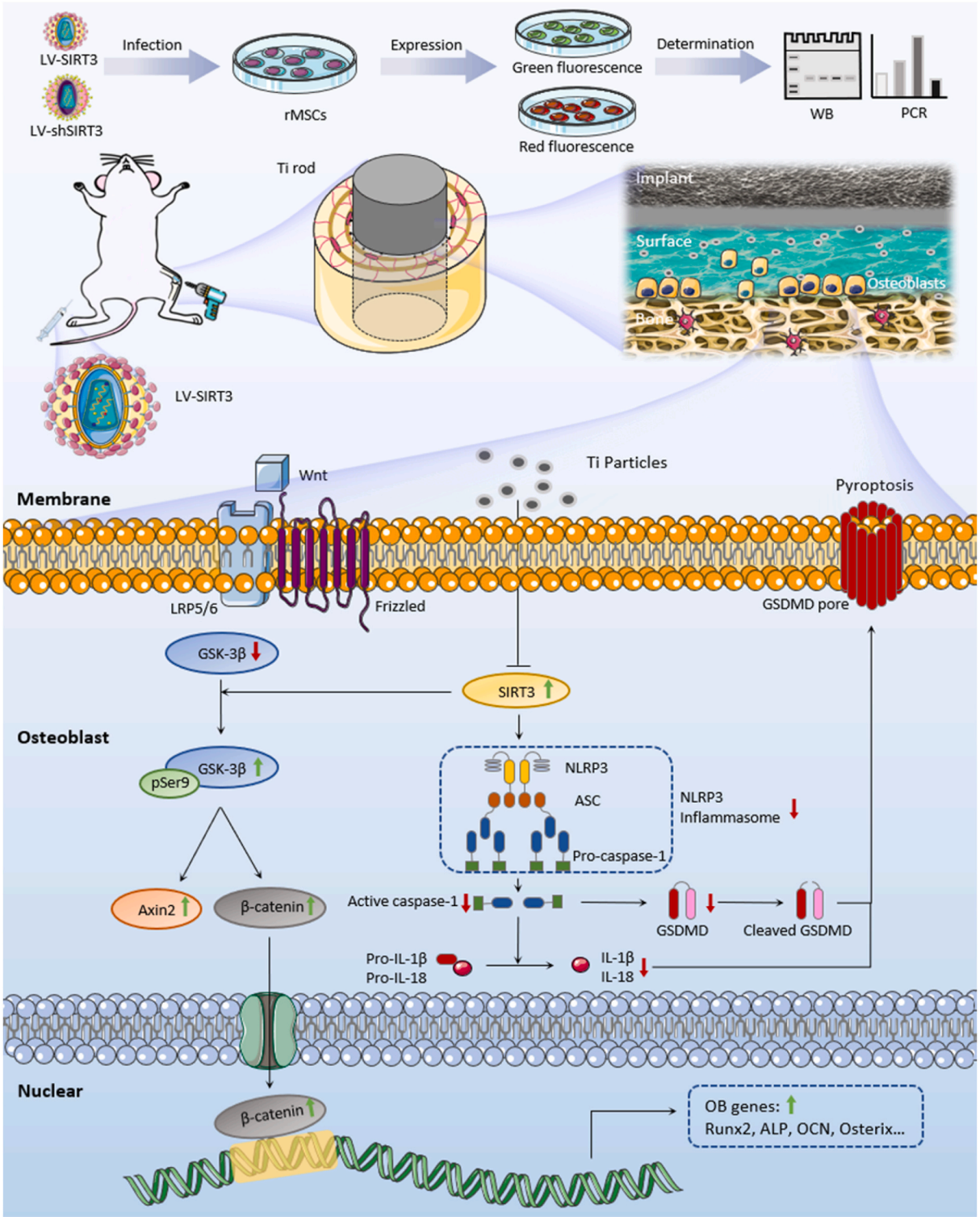

Scheme 1. Schematic illustration of this work. SIRT3 is known to possess an NAD^+-dependent protein deacetylase located in mitochondria. Lentiviral transduction efficiency in cells with LV-shSIRT3 or LV-SIRT3 was determined by fluorescence microscopy, Western blot and qRT-PCR analyses. Ti particle-induced bone loss surrounding the implant was inhibited by upregulating the expression of SIRT3 to mitigate osteogenic reduction through the inhibition of the NLRP3 inflammasome and downstream proinflammatory cytokines via the GSK-3β/β-catenin signalling pathway.

draft. **Jiaxiang Bai:** Writing – review & editing. **Ning Li:** Methodology, Data curation. **Meng Li:** Software, Formal analysis, Methodology. **Houyi Sun:** Methodology. **Weicheng Zhang:** Formal analysis. **Gaoran Ge:** Data curation. **Xiaolong Liang:** Validation. **Huaqiang Tao:** Data curation. **Yi Xue:** Data curation. **Yuefeng Hao:** Supervision. **Chen Zhu:** Supervision. **Yaozeng Xu:** Supervision, Conceptualization. **Dechun Geng:** Project administration, Supervision, Writing – review & editing.

Declaration of competing interest

The authors declare that they have no known competing financial interests or personal relationships that could have appeared to influence

the work reported in this paper.

Acknowledgements

This work is supported by grants from the National Natural Science Foundation of China (Nos. 82072425, 82072498, 81873991, 81873990, 81672238 and 81472077), the Young Medical Talents of Jiangsu Province (No. QNRC2016751), the Natural Science Foundation of Jiangsu Province (Nos. BK20180001), the Priority Academic Program Development of Jiangsu Higher Education Institutions and Special Project of Diagnosis and Treatment Technology for Key Clinical Diseases in Suzhou (LCZX202003).

Appendix A. Supplementary data

Supplementary data to this article can be found online at https://doi.org/10.1016/j.bioactmat.2021.02.039.

References

[1] P.F. Sharkey, P.M. Lichstein, C. Shen, A.T. Tokarski, J. Parvizi, Why are total knee arthroplasties failing today-has anything changed after 10 years? J. Arthroplasty 29 (9) (2014) 1774–1778, https://doi.org/10.1016/j.arth.2013.07.024.

[2] Australian Orthopaedic Association National Joint Replacement Registry (AOANJRR), Hip, Knee & Shoulder Arthroplasty: 2019 Annual Report, AOA, Adelaide, 2019, pp. 1–436 [Accessed from: https://aoanjrr.sahmri.com/annual-reports-2019.

[3] R.E. Delanois, J.B. Mistry, C.U. Gwam, N.S. Mohamed, U.S. Choksi, M.A. Mont, Current epidemiology of revision total knee arthroplasty in the United States, J. Arthroplasty 32 (9) (2017) 2663–2668, https://doi.org/10.1016/j.arth.2017.03.066.

[4] S.B. Goodman, Wear particles, periprosthetic osteolysis and the immune system, Biomaterials 28 (34) (2007) 5044–5048, https://doi.org/10.1016/j.biomaterials.2007.06.035.

[5] B. Li, Y. Hu, Y. Zhao, M. Cheng, H. Qin, T. Cheng, Q. Wang, X. Peng, X. Zhang, Curcumin attenuates titanium particle-induced inflammation by regulating macrophage polarization in vitro and in vivo, Front. Immunol. 8 (2017) 55, https://doi.org/10.3389/fimmu.2017.00055.

[6] N. Liu, J. Meng, Z. Wang, G. Zhou, T. Shi, J. Zhao, Autophagy mediated TiAl(6)V(4) particle-induced peri-implant osteolysis by promoting expression of TNF-alpha, Biochem. Biophys. Res. Commun. 473 (1) (2016) 133–139, https://doi.org/10.1016/j.bbrc.2016.03.065.

[7] Y. Kadoya, P.A. Revell, N. al-Saffar, A. Kobayashi, G. Scott, M.A. Freeman, Bone formation and bone resorption in failed total joint arthroplasties: histomorphometric analysis with histochemical and immunohistochemical technique, J. Orthop. Res. 14 (3) (1996) 473–482, https://doi.org/10.1002/jor.1100140318.

[8] J.C. Clohisy, T. Hirayama, E. Frazier, S.K. Han, Y. Abu-Amer, NF-kB signaling blockade abolishes implant particle-induced osteoclastogenesis, J. Orthop. Res. 22 (1) (2004) 13–20, https://doi.org/10.1016/S0736-0266(03)00156-6.

[9] J.A. Kim, H.J. Ihn, J.Y. Park, J. Lim, J.M. Hong, S.H. Kim, S.Y. Kim, H.I. Shin, E. K. Park, Inhibitory effects of triptolide on titanium particle-induced osteolysis and receptor activator of nuclear factor-kappaB ligand-mediated osteoclast differentiation, Int. Orthop. 39 (1) (2015) 173–182, https://doi.org/10.1007/s00264-014-2596-3.

[10] B. Tian, T. Jiang, Z. Shao, Z. Zhai, H. Li, Q. Fan, X. Liu, Z. Ouyang, T. Tang, Q. Jiang, M. Zheng, K. Dai, A. Qin, Y. Yu, Z. Zhu, The prevention of titanium-particle-induced osteolysis by OA-14 through the suppression of the p38 signaling pathway and inhibition of osteoclastogenesis, Biomaterials 35 (32) (2014) 8937–8950, https://doi.org/10.1016/j.biomaterials.2014.06.055.

[11] E.D. Deeks, Denosumab: a review in postmenopausal osteoporosis, Drugs Aging 35 (2) (2018) 163–173, https://doi.org/10.1007/s40266-018-0525-7.

[12] S.R. Cummings, J. San Martin, M.R. McClung, E.S. Siris, R. Eastell, I.R. Reid, P. Delmas, H.B. Zoog, M. Austin, A. Wang, S. Kutilek, S. Adami, J. Zanchetta, C. Libanati, S. Siddhanti, C. Christiansen, F. Trial, Denosumab for prevention of fractures in postmenopausal women with osteoporosis, N. Engl. J. Med. 361 (8) (2009) 756–765, https://doi.org/10.1056/NEJMoa0809493.

[13] B.H. Ahn, H.S. Kim, S. Song, I.H. Lee, J. Liu, A. Vassilopoulos, C.X. Deng, T. Finkel, A role for the mitochondrial deacetylase Sirt3 in regulating energy homeostasis, Proc. Natl. Acad. Sci. U. S. A. 105 (38) (2008) 14447–14452, https://doi.org/10.1073/pnas.0803790105.

[14] K. Leuner, T. Schutt, C. Kurz, S.H. Eckert, C. Schiller, A. Occhipinti, S. Mai, M. Jendrach, G.P. Eckert, S.E. Kruse, R.D. Palmiter, U. Brandt, S. Drose, I. Wittig, M. Willem, C. Haass, A.S. Reichert, W.E. Muller, Mitochondrion-derived reactive oxygen species lead to enhanced amyloid beta formation, Antioxidants Redox Signal. 16 (12) (2012) 1421–1433, https://doi.org/10.1089/ars.2011.4173.

[15] S.J. Allison, J. Milner, SIRT3 is pro-apoptotic and participates in distinct basal apoptotic pathways, Cell Cycle 6 (21) (2007) 2669–2677, https://doi.org/10.4161/cc.6.21.4866.

[16] J.E. Huh, J.H. Shin, E.S. Jang, S.J. Park, D.R. Park, R. Ko, D.H. Seo, H.S. Kim, S. H. Lee, Y. Choi, H.S. Kim, S.Y. Lee, Sirtuin 3 (SIRT3) maintains bone homeostasis by regulating AMPK-PGC-1beta axis in mice, Sci. Rep. 6 (2016), 22511, https://doi.org/10.1038/srep22511.

[17] H. Kim, Y.D. Lee, H.J. Kim, Z.H. Lee, H.H. Kim, SOD2 and Sirt3 control osteoclastogenesis by regulating mitochondrial ROS, J. Bone Miner. Res. 32 (2) (2017) 397–406, https://doi.org/10.1002/jbmr.2974.

[18] Y. Ding, H. Yang, Y. Wang, J. Chen, Z. Ji, H. Sun, Sirtuin 3 is required for osteogenic differentiation through maintenance of PGC-1a-SOD2-mediated regulation of mitochondrial function, Int. J. Biol. Sci. 13 (2) (2017) 254–264, https://doi.org/10.7150/ijbs.17053.

[19] Y. He, H. Hara, G. Nunez, Mechanism and regulation of NLRP3 inflammasome activation, Trends Biochem. Sci. 41 (12) (2016) 1012–1021, https://doi.org/10.1016/j.tibs.2016.09.002.

[20] Y. Yang, H. Wang, M. Kouadir, H. Song, F. Shi, Recent advances in the mechanisms of NLRP3 inflammasome activation and its inhibitors, Cell Death Dis. 10 (2) (2019) 128, https://doi.org/10.1038/s41419-019-1413-8.

[21] T. Strowig, J. Henao-Mejia, E. Elinav, R. Flavell, Inflammasomes in health and disease, Nature 481 (7381) (2012) 278–286, https://doi.org/10.1038/nature10759.

[22] G. Mbalaviele, D.V. Novack, G. Schett, S.L. Teitelbaum, Inflammatory osteolysis: a conspiracy against bone, J. Clin. Invest. 127 (6) (2017) 2030–2039, https://doi.org/10.1172/JCI93356.

[23] L. Burton, D. Paget, N.B. Binder, K. Bohnert, B.J. Nestor, T.P. Sculco, L. Santambrogio, F.P. Ross, S.R. Goldring, P.E. Purdue, Orthopedic wear debris mediated inflammatory osteolysis is mediated in part by NALP3 inflammasome activation, J. Orthop. Res. 31 (1) (2013) 73–80, https://doi.org/10.1002/jor.22190.

[24] J. Traba, M. Kwarteng-Siaw, T.C. Okoli, J. Li, R.D. Huffstutler, A. Bray, M. A. Waclawiw, K. Han, M. Pelletier, A.A. Sauve, R.M. Siegel, M.N. Sack, Fasting and refeeding differentially regulate NLRP3 inflammasome activation in human subjects, J. Clin. Invest. 125 (12) (2015) 4592–4600, https://doi.org/10.1172/JCI83260.

[25] D. Geng, Y. Xu, H. Yang, J. Wang, X. Zhu, G. Zhu, X. Wang, Protection against titanium particle induced osteolysis by cannabinoid receptor 2 selective antagonist, Biomaterials 31 (8) (2010) 1996–2000, https://doi.org/10.1016/j.biomaterials.2009.11.069.

[26] Y. Huang, X. Jia, K. Bai, X. Gong, Y. Fan, Effect of fluid shear stress on cardiomyogenic differentiation of rat bone marrow mesenchymal stem cells, Arch. Med. Res. 41 (7) (2010) 497–505, https://doi.org/10.1016/j.arcmed.2010.10.002.

[27] S.B. Goodman, J. Gallo, Periprosthetic osteolysis: mechanisms, prevention and treatment, J. Clin. Med. 8 (12) (2019), https://doi.org/10.3390/jcm8122091.

[28] P.E. Purdue, P. Koulouvaris, H.G. Potter, B.J. Nestor, T.P. Sculco, The cellular and molecular biology of periprosthetic osteolysis, Clin. Orthop. Relat. Res. 454 (2007) 251–261, https://doi.org/10.1097/01.blo.0000238813.95035.1b.

[29] S.B. Goodman, T. Ma, R. Chiu, R. Ramachandran, R.L. Smith, Effects of orthopaedic wear particles on osteoprogenitor cells, Biomaterials 27 (36) (2006) 6096–6101, https://doi.org/10.1016/j.biomaterials.2006.08.023.

[30] N.J. German, M.C. Haigis, Sirtuins and the metabolic hurdles in cancer, Curr. Biol. 25 (13) (2015) R569–R583, https://doi.org/10.1016/j.cub.2015.05.012.

[31] W. Yang, K. Nagasawa, C. Munch, Y. Xu, K. Satterstrom, S. Jeong, S.D. Hayes, M. P. Jedrychowski, F.S. Vyas, E. Zaganjor, V. Guarani, A.E. Ringel, S.P. Gygi, J. W. Harper, M.C. Haigis, Mitochondrial sirtuin network reveals dynamic SIRT3-dependent deacetylation in response to membrane depolarization, Cell 167 (4) (2016) 985–1000, https://doi.org/10.1016/j.cell.2016.10.016, e21.

[32] H. Pi, S. Xu, R.J. Reiter, P. Guo, L. Zhang, Y. Li, M. Li, Z. Cao, L. Tian, J. Xie, R. Zhang, M. He, Y. Lu, C. Liu, W. Duan, Z. Yu, Z. Zhou, SIRT3-SOD2-mROS-dependent autophagy in cadmium-induced hepatotoxicity and salvage by melatonin, Autophagy 11 (7) (2015) 1037–1051, https://doi.org/10.1080/15548627.2015.1052208.

[33] E. McDonnell, B.S. Peterson, H.M. Bomze, M.D. Hirschey, SIRT3 regulates progression and development of diseases of aging, Trends Endocrinol. Metabol. 26 (9) (2015) 486–492, https://doi.org/10.1016/j.tem.2015.06.001.

[34] A. Chalkiadaki, L. Guarente, The multifaceted functions of sirtuins in cancer, Nat. Rev. Canc. 15 (10) (2015) 608–624, https://doi.org/10.1038/nrc3985.

[35] D. Kurundkar, A.R. Kurundkar, N.B. Bone, E.J. Becker Jr., W. Liu, B. Chacko, V. Darley-Usmar, J.W. Zmijewski, V.J. Thannickal, SIRT3 diminishes inflammation and mitigates endotoxin-induced acute lung injury, JCI Insight 4 (1) (2019), https://doi.org/10.1172/jci.insight.120722.

[36] W.Y. Zhao, L. Zhang, M.X. Sui, Y.H. Zhu, L. Zeng, Protective effects of sirtuin 3 in a murine model of sepsis-induced acute kidney injury, Sci. Rep. 6 (2016), 33201, https://doi.org/10.1038/srep33201.

[37] N.R. Sundaresan, M. Gupta, G. Kim, S.B. Rajamohan, A. Isbatan, M.P. Gupta, Sirt3 blocks the cardiac hypertrophic response by augmenting Foxo3a-dependent antioxidant defense mechanisms in mice, J. Clin. Invest. 119 (9) (2009) 2758–2771, https://doi.org/10.1172/JCI39162.

[38] J. Zheng, L. Shi, F. Liang, W. Xu, T. Li, L. Gao, Z. Sun, J. Yu, J. Zhang, Sirt3 ameliorates oxidative stress and mitochondrial dysfunction after intracerebral hemorrhage in diabetic rats, Front. Neurosci. 12 (2018) 414, https://doi.org/10.3389/fnins.2018.00414.

[39] Y. Naganuma, Y. Takakubo, T. Hirayama, Y. Tamaki, J. Pajarinen, K. Sasaki, S. B. Goodman, M. Takagi, Lipoteichoic acid modulates inflammatory response in macrophages after phagocytosis of titanium particles through Toll-like receptor 2 cascade and inflammasomes, J. Biomed. Mater. Res. 104 (2) (2016) 435–444, https://doi.org/10.1002/jbm.a.35581.

[40] S.H. McCall, M. Sahraei, A.B. Young, C.S. Worley, J.A. Duncan, J.P. Ting, I. Marriott, Osteoblasts express NLRP3, a nucleotide-binding domain and leucine-rich repeat region containing receptor implicated in bacterially induced cell death, J. Bone Miner. Res. 23 (1) (2008) 30–40, https://doi.org/10.1359/jbmr.071002.

[41] L. Wang, K. Chen, X. Wan, F. Wang, Z. Guo, Z. Mo, NLRP3 inflammasome activation in mesenchymal stem cells inhibits osteogenic differentiation and enhances adipogenic differentiation, Biochem. Biophys. Res. Commun. 484 (4) (2017) 871–877, https://doi.org/10.1016/j.bbrc.2017.02.007.

[42] J.B. Kim, P. Leucht, K. Lam, C. Luppen, D. Ten Berge, R. Nusse, J.A. Helms, Bone regeneration is regulated by wnt signaling, J. Bone Miner. Res. 22 (12) (2007) 1913–1923, https://doi.org/10.1359/jbmr.070802.

[43] T. Yodthong, U. Kedjarune-Leggat, C. Smythe, R. Wititsuwannakul, T. Pitakpornpreecha, l-quebrachitol promotes the proliferation, differentiation, and mineralization of MC3T3-E1 cells: involvement of the BMP-2/Runx2/MAPK/Wnt/beta-catenin signaling pathway, Molecules 23 (12) (2018), https://doi.org/10.3390/molecules23123086.

[44] L. Pederson, M. Ruan, J.J. Westendorf, S. Khosla, M.J. Oursler, Regulation of bone formation by osteoclasts involves Wnt/BMP signaling and the chemokine sphingosine-1-phosphate, Proc. Natl. Acad. Sci. U. S. A. 105 (52) (2008) 20764–20769, https://doi.org/10.1073/pnas.0805133106.

[45] Y. Gu, Z. Wang, J. Shi, L. Wang, Z. Hou, X. Guo, Y. Tao, X. Wu, W. Zhou, Y. Liu, W. Zhang, Y. Xu, H. Yang, F. Xue, D. Geng, Titanium particle-induced osteogenic inhibition and bone destruction are mediated by the GSK-3beta/beta-catenin signal pathway, Cell Death Dis. 8 (6) (2017), e2878, https://doi.org/10.1038/cddis.2017.275.

[46] L. Li, M. Yu, Y. Li, Q. Li, H. Yang, M. Zheng, Y. Han, D. Lu, S. Lu, L. Gui, Synergistic anti-inflammatory and osteogenic n-HA/resveratrol/chitosan composite microspheres for osteoporotic bone regeneration, Bioact. Mater. 6 (5) (2021) 1255–1266, https://doi.org/10.1016/j.bioactmat.2020.10.018.

[47] A.M. Boniakowski, A.D. denDekker, F.M. Davis, A. Joshi, A.S. Kimball, M. Schaller, R. Allen, J. Bermick, D. Nycz, M.E. Skinner, S. Robinson, A.T. Obi, B.B. Moore, J. E. Gudjonsson, D. Lombard, S.L. Kunkel, K.A. Gallagher, SIRT3 regulates macrophage-mediated inflammation in diabetic wound repair, J. Invest. Dermatol. 139 (12) (2019) 2528–2537, https://doi.org/10.1016/j.jid.2019.05.017, e2.